Electrode Performance in Reversible Solid Oxide Fuel Cells

O. A. Marina,[a,*,z] **L. R. Pederson,**[a] **M. C. Williams,**[b,**] **G. W. Coffey,**[a,*]
K. D. Meinhardt,[a] **C. D. Nguyen,**[a] **and E. C. Thomsen**[a]

[a]*Pacific Northwest National Laboratory, Richland, Washington 99352 USA*
[b]*National Energy Technology Laboratory, Morgantown, West Virginia 26507, USA*

The performance of several negative (fuel) and positive (air) electrode compositions for use in reversible solid oxide fuel cells capable of operating both as a fuel cell and as an electrolyzer was investigated in half-cell and full-cell tests. Negative electrode compositions studied were a nickel/zirconia cermet (Ni/YSZ) and lanthanum-substituted strontium titanate/ceria composite, whereas positive electrode compositions examined included mixed ion- and electron-conducting lanthanum strontium ferrite (LSF), lanthanum strontium copper ferrite (LSCuF), lanthanum strontium cobalt ferrite (LSCoF), and lanthanum strontium manganite (LSM). While titanate/ceria and Ni/YSZ electrodes performed similarly in the fuel cell mode in half-cell tests, losses associated with electrolysis were lower for the titanate/ceria electrode. Positive electrodes gave generally higher losses in the electrolysis mode when compared to the fuel cell mode. This behavior was most apparent for mixed-conducting LSCuF and LSCoF electrodes, and discernible but smaller for LSM; observations were consistent with expected trends in the interfacial oxygen vacancy concentration under anodic and cathodic polarization. Full-cell tests conducted for cells with a thin electrolyte (7 μm YSZ) similarly showed higher polarization losses in the electrolysis than fuel cell direction.
© 2007 The Electrochemical Society. [DOI: 10.1149/1.2710209] All rights reserved.

Electrolysis has long been used to dissociate water into its constituents of oxygen and hydrogen. Various electrolyzers have been developed and are commercially available today, including those based on proton exchange membranes, molten carbonate, phosphoric acid, alkaline, and solid oxide technology.[1-5] Some of these are reversible systems capable of operating both as a fuel cell and as an electrolyzer, although fuel cell and electrolyzer functions are carried out in separate subsystems. A reversible fuel cell can take advantage of excess electrical grid capacity during off-peak hours to produce hydrogen fuel, to be utilized later during periods of high electrical demand. The power unit (fuel cell) is sized for the peaking load in a practical reversible fuel cell, whereas the electrolyzer is rated at a power that can produce sufficient hydrogen to recharge the hydrogen storage capacity over the remaining hours of the day. If energy conversion, electrical to chemical and chemical to electrical, can occur in the same device with reasonable efficiencies, there could be significant overall cost benefits.

For solid oxide electrolysis cells (SOEC) to be of commercial interest, the cost of the hydrogen produced must be competitive with that of other means of production. The cost of electricity is a significant factor in steam electrolysis, comprising 75% to 95% of that of electrolysis-derived hydrogen according to performance and cost targets established by the U.S. Department of Energy, depending on the scale of the plant.[5] Electrical energy requirements could be lessened if waste heat was available, such as from nuclear plants.[6] However, the ability to utilize waste heat in an SOEC is affected by the fact that endothermic steam decomposition is at least partially offset by ohmic heating within the cell. The thermal efficiency, η_t, of a steam electrolyzer is defined as[7]

$$\eta_t = \frac{-\Delta \bar{h}_f/2F}{E} \qquad [1]$$

where $\Delta \bar{h}_f$ is the enthalpy of formation, F is the Faraday constant, and E is the cell potential, whereas the thermal efficiency of a solid oxide fuel cell (SOFC) is the inverse of Eq. 1. The net reaction in an SOEC would be endothermic if operated at potentials below the thermal neutral point ($V_{thermal\ neutral} = -\Delta \bar{h}_f/2F = 1.29$ V at 850°C, where $\eta_t = 1$), and exothermic if operated above that potential.[8] Dönitz et al.[9-13] found that ohmic heating was sufficient to sustain high-temperature steam electrolysis in cells operated at potentials

greater than $V_{thermal\ neutral}$, which may be advantageous especially for small-scale electrolyzers. A reduction in operating cell potentials as a means of improving efficiency of steam electrolyzers has been suggested,[4] where heat from nonelectrical sources could be more effectively utilized.

While previous studies have shown that reversible fuel cell operation is certainly feasible, differences in performance in the fuel cell vs electrolysis direction has been reported. Eguchi et al.[14] found that a Ni/yttria-stablized zirconia (YSZ) negative electrode and a lanthanum strontium manganite (LSM) positive electrode combination performed better as an SOFC than as an SOEC, while a platinum negative electrode combined with a LSCo positive electrode gave lower polarization losses as an SOEC than as an SOFC. Momma et al.[15] similarly found that Ni/YSZ was less active as the negative electrode in an SOEC than in an SOFC, and attributed this behavior to the contribution of a diffusion-limited process in the electrolysis direction. Hauch et al.[16] found that a Ni/YSZ negative electrode was susceptible to aging in a high-steam environment, primarily due to coarsening of nickel particles. In that study, polarization losses due to the Ni/YSZ electrode nearly doubled when exposed to a 2/98 hydrogen/steam mixture at 850°C, with a characteristic time constant of 38 h. Jacobsen et al.[17] reported significant nonlinear behavior for a Pt/YSZ positive electrode under cathodic vs anodic polarization, finding that the electrode was considerably more active for oxygen ion oxidation than for oxygen reduction. Furthermore, steady-state currents were achieved rapidly with anodic polarization, but only very slowly with cathodic polarization. Svensson et al.[18] have developed a model for mixed-conducting perovskite air electrodes on a zirconia electrolyte that predicts Tafel-like behavior under cathodic polarization, and a limiting current under anodic polarization. Limiting current behavior under anodic polarization was attributed to a depletion of oxygen vacancies at the electrode/electrolyte interface. A recent study by O'Brien et al.,[19] however, found little difference between area specific resistance values in fuel cell and electrolysis directions for an electrolyte-supported single cell with a Ni/YSZ negative electrode and an LSM positive electrode.

The purpose of this study was to compare inefficiencies associated with electrode reactions when operated in SOFC and SOEC modes. Especially for Ni/YSZ-supported cells with very thin (<10 μm) electrolyte layers, electrode processes were expected to dominate cell performance in both directions. Negative electrode compositions that were studied included Ni/YSZ and lanthanum strontium titanate/ceria composites, while positive electrode compositions considered included LSF, LSCuF, LSCoF, and LSM. Rare earth-substituted strontium titanate is an n-type semiconductor under
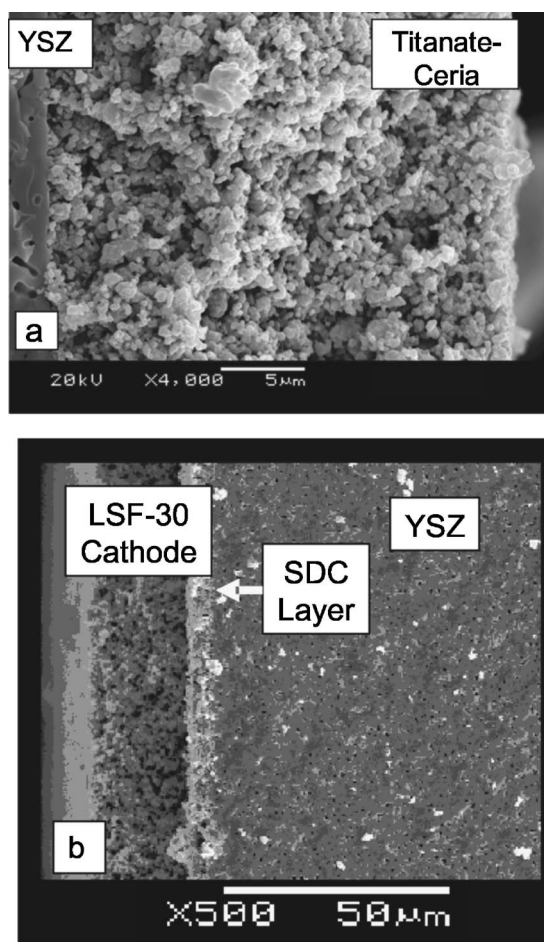
Figure 1. Scanning electron micrographs of (a) titanate/ceria ($La_{0.35}Sr_{0.65}TiO_3$ + $Ce_{0.5}La_{0.5}O_{2-\delta}$) and (b) $La_{0.80}Sr_{0.20}FeO_{3-\delta}$ electrodes sintered onto an 8YSZ electrolyte.

Figure 2. (Color online) Schematic electrochemical cell incorporating the working electrode (WE), counter electrode (CE), and a Luggin-type Pt reference electrode (RE). In positive electrode studies air was fed to the working electrode.

reducing conditions present at the negative electrode side.[20-25] Advantages of these materials as an SOFC anode includes stability when exposed to oxygen and tolerance to sulfur compounds.[25,26] Furthermore, ceria-modified strontium titanate negative electrodes were shown to have much improved electrocatalytic activity toward hydrogen.[25] The modest electrical conductivity of the ceria phase was enhanced through partial substitution with lanthanum, as has been described previously.[20,27] It is not excluded that a small fraction of any of these may have substituted into the titanate phase as well, although it was impossible to detect using standard X-ray diffraction (XRD) techniques. Positive electrode compositions LSF, LSCuF, and LSCoF were mixed electron- and ion-conducting materials that generally show lower overpotential losses in an SOFC compared to the baseline cathode LSM,[28-36] though may be less stable.

Experimental

Positive and negative electrode materials were prepared by glycine nitrate combustion synthesis.[37] The titanate/ceria electrode composition was $La_{0.35}Sr_{0.65}TiO_3$-$Ce_{0.5}La_{0.5}O_{2-\delta}$ in a 5:5 ratio. Titanate/ceria composite powder was calcined at 1200°C for 1 h, attrition milled, and sieved to −325 mesh. Electrode inks were prepared by mixing the calcined oxide powders with a commercial screen-printing binder in a three-roll mill until uniform. Negative electrode inks were screened onto 8 mole percent YSZ pellets (16 mm diam, 3 mm thick) and sintered at 1000°C for 2 h. The resulting electrodes were ∼15–20 μm in thickness, with 30–40% porosity. A typical sintered microstructure of the titanate/ceria com-
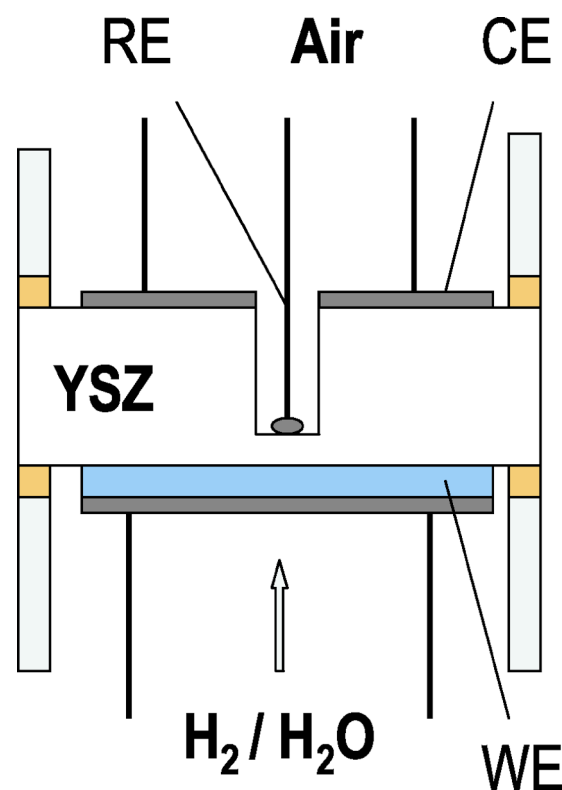
posite electrode on a YSZ electrolyte is given in Fig. 1a. Ni-YSZ electrodes were prepared from a NiO-YSZ mixture in a similar fashion and sintered at 1375°C for 2 h in air. The electrode contained 50 vol % of Ni after reduction. Reduction was performed in the experimental setup in situ during sealing at 950°C. Representative positive electrode compositions included in this study were $La_{0.80}Sr_{0.20}FeO_{3-\delta}$ (LSF-20), $La_{0.70}Sr_{0.30}Cu_{0.10}Fe_{0.90}O_{3-\delta}$ (LSCuF-7319), $La_{0.60}Sr_{0.40}Co_{0.20}Fe_{0.80}O_{3-\delta}$ (LSCoF-6428), and $La_{0.80}Sr_{0.20}MnO_{3-\delta}$ (LSM-20). The positive electrode powders were calcined for 1 h at 1000°C, attrition-milled, and screened to achieve an average particle size of 0.5 to 1 μm. The positive electrodes were screen-printed onto an YSZ pellet with a presintered <5 μm thick 20 mol % samaria-doped ceria (SDC) interlayer, and sintered at 1200°C for 2 h for LSF-20, LSM-20, and LSCoF-6428 electrodes and at 900°C for 1 h for LSCuF-7319 electrodes. As an example, a scanning electron micrograph of the LSF cathode is given in Fig. 1b.

Electrode overpotentials for positive and negative electrodes were determined as a function of current density under both anodic and cathodic polarization. An internal, Luggin-type reference electrode was used, consisting of a Pt/PtO or Pt/Ag/AgO reference wire (negative and positive electrode study, respectively) placed in a blind hole drilled halfway through the YSZ pellet, shown in Fig. 2. This geometry is the preferred reference electrode configuration as it accurately measures both electrolyte and electrode impedances.[38] Electrode overpotentials were measured for both the negative and positive electrode by current interrupt methods at a scan rate of 1 mV/s using a Solartron 1260/1287 potentiostat/galvanostat. Negative electrode measurements were performed in a mixture of hydrogen, steam, and nitrogen, while positive electrode studies were performed in air.

An anode-supported SOFC cell with an active area of 33.6 cm² was constructed, following that described previously.[39] The negative electrode was a Ni/YSZ composite, with a total thickness of
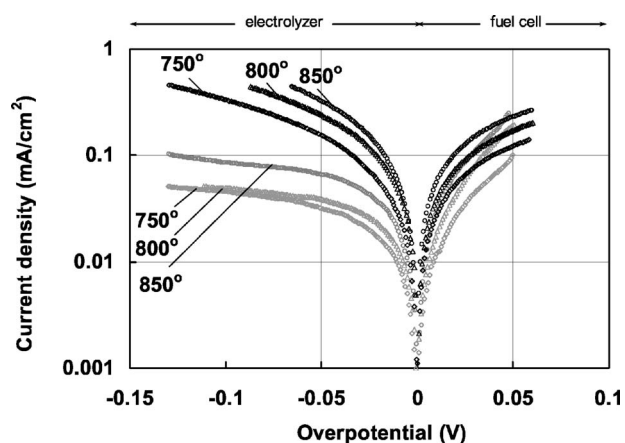
Figure 3. Current-overpotential dependencies obtained on Ni-YSZ (gray symbols) and ceramic composite $La_{0.35}Sr_{0.65}TiO_{3-\delta}$-$Ce_{0.5}La_{0.5}O_{1.75-\delta}$ (black symbols) electrodes at 750–850°C and H_2/H_2O = 50/50.

Figure 5. (Color online) Current-overpotential dependencies obtained on Ni-YSZ and ceramic $La_{0.35}Sr_{0.65}TiO_{3-\delta}$-$Ce_{0.5}La_{0.5}O_{1.75-\delta}$ electrodes at 800°C at a constant p_{H_2} = 0.1 atm and varied p_{H_2O}.

550 μm and with 40 vol % nickel present after reduction. The active electrode layer was about 5 μm thick and had 50 vol % nickel after reduction. The electrolyte was 8YSZ, ~7 μm in thickness. A 2 μm thick SDC barrier layer was applied to the presintered anode/electrolyte structure by screen printing, followed by the application of a 30 μm thick cathode consisting of LSCoF-6428. Steam concentrations in the SOEC mode were varied from 10 to 90%, with a balance of hydrogen. Tests in the SOFC mode were performed using hydrogen saturated with water at room temperature (ca. 3 percent steam).

Results and Discussion

Negative (fuel) electrode polarization studies.— Polarization losses associated with nickel/zirconia and titanate/ceria composite electrodes were evaluated under conditions typical of fuel cell and electrolyzer operation and are given in Fig. 3-6. Figure 3 shows polarization losses of the Ni/YSZ and electrode composed of $La_{0.35}Sr_{0.65}TiO_3$-$Ce_{0.5}La_{0.5}O_{1.75-\delta}$ at 750, 800, and 850°C in a mixture of 50% hydrogen and 50% water. Both electrodes performed similarly in the fuel cell mode. Using a constant polarization loss of 50 mV at 800°C for purposes of comparison in half-cell measurements, an area specific resistance of 0.29 Ω-cm² was calculated for the titanate/ceria and 0.26 Ω-cm² for the Ni/YSZ electrode, when operated as a fuel cell. When operated as an electrolyzer, the
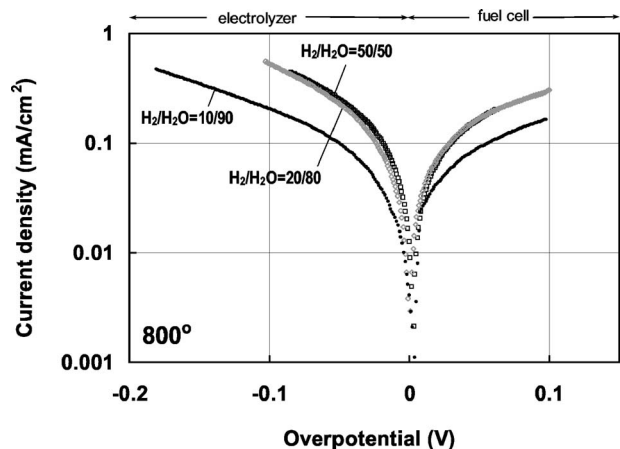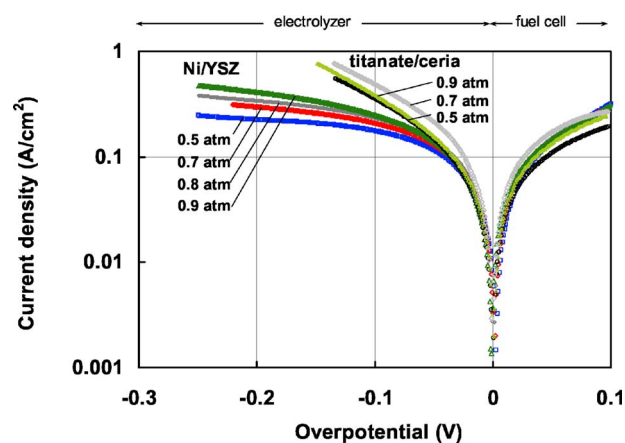
titanate/ceria composite negative electrodes performed somewhat better than Ni/YSZ: at 800°C the titanate/ceria and Ni/YSZ electrodes showed area specific polarization resistances of 0.21 and 0.29 Ω-cm², respectively, in the same gas mixture and a polarization loss of 50 mV. As expected, higher temperatures favored performances of both electrodes for both hydrogen oxidation and steam electrolysis. In this temperature range, the titanate/ceria electrode showed slightly higher activity for steam electrolysis than for hydrogen oxidation, while the Ni/YSZ electrode exhibited higher activity for hydrogen oxidation than steam electrolysis. The latter is in agreement with results reported by Eguchi et al.[14] and by Momma et al.:[15] polarization curves of Ni/YSZ show asymmetric behavior for hydrogen oxidation and water electrolysis.

It is emphasized that the Ni/YSZ powder composition and electrode sintering conditions applied in this work, and therefore electrode microstructures, were identical to those used for the fabrication of the SOFC anode functional layer in anode-supported cells.[39] The only difference was the absence of the thick Ni/YSZ current collecting layer in cells used in half cell measurements. The functional layer of Ni/YSZ electrodes utilized in the present study were 20–30 μm thick; very thin Ni/YSZ (<10 μm) electrodes tended to degrade more rapidly at high p_{H_2O} than did the thicker structures. Electrode degradation might be ascribed to the Ni particles agglomeration followed by a decrease in the length of the triple phase boundary where the electrochemical reaction is believed to take place. It is well known that sintering of Ni particles is accelerated in
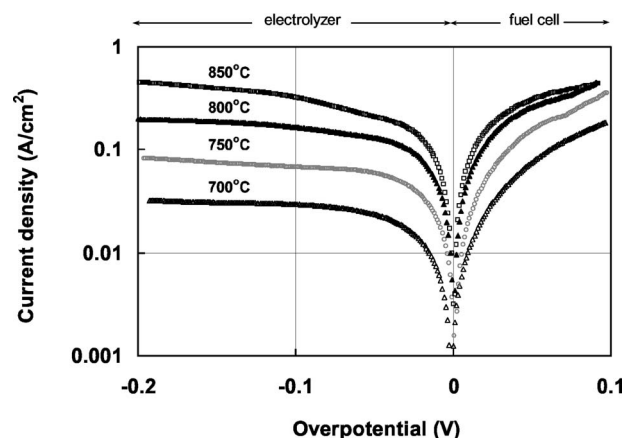

Figure 4. Current-overpotential dependencies obtained on ceramic $La_{0.35}Sr_{0.65}TiO_{3-\delta}$-$Ce_{0.5}La_{0.5}O_{1.75-\delta}$ electrode at 800°C at H_2/H_2O = 50/50, 20/80, and 10/90.

Figure 6. Current-overpotential dependencies obtained on Ni-YSZ electrode at $H_2/H_2O/N_2$ = 10/70/20 in the temperature range 700–850°C.

the presence of steam.[40] It is possible that thin electrodes are more susceptible to coarsening than thicker ones. Note that no similar effect was noticed for the titanate/ceria electrodes; oxide particles are not expected to be agglomerating the way metal particles do.

An increase in a steam-to-hydrogen ratio from 50/50 to 80/20 at 800°C did not affect polarization losses for the titanate/ceria in either the electrolyzer or fuel cell modes, as shown in Fig. 4. However, when the H_2O/H_2 was further increased to 90/10, the electrode performance decreased. This could be potentially understood in terms of the titanate/ceria conductivity and its dependence on a p_{O_2}. As shown in Ref. 41, the conductivity of titanate/ceria composites similar in composition to those of this study decreases with increasing p_{O_2}. When switching from a $H_2O/H_2 = 50/50$ to $H_2O/H_2 = 90/10$, the oxygen partial pressure changes by almost two orders of magnitude, from 4×10^{-19} atm to 3×10^{-17} atm, thereby affecting both electrical conductivity and electrode performance.

The dependence of electrode polarization losses on the steam partial pressure was investigated in both fuel cell and electrolyzer modes. Figure 5 gives current-overpotential dependencies obtained for the Ni/YSZ and titanate/ceria composite electrodes at 800°C at a constant partial pressure of hydrogen of 0.1 atm and partial pressures of water ranging from 0.5 to 0.9 atm. All data reported here was obtained after at least 5 h of exposure to a new p_{H_2O} to assure an electrode steady-state was achieved. As seen in Fig. 5, polarization losses associated with the hydrogen oxidation reaction (the fuel cell mode) were similar for both electrodes. When considering a constant polarization loss of 0.1 V, electrode polarization resistances at 800°C were around 0.32 Ω-cm^2. When operating as an electrolyzer, area-specific resistances of the Ni/YSZ electrode were higher than those obtained when operated as a fuel cell at the same polarization loss. It is also seen in Fig. 5 that performances of both electrodes were more strongly affected by increases in the partial pressure of water when operated as an electrolyzer than as a fuel cell. Polarization losses decreased with increased concentration of water in the electrolysis mode. This was more pronounced with the Ni/YSZ electrode: when p_{H_2O} was increased from 0.5 to 0.9 atm, the polarization resistance of Ni/YSZ decreased from 0.56 to 0.40 Ω-cm^2. When the titanate/ceria electrode was operated in the electrolysis mode, the area specific resistances decreased to 0.20–0.28 Ω-cm^2 at a constant polarization loss of 0.1 V in the p_{H_2O} range 0.5–0.9 atm. As illustrated in Fig. 6 for the Ni/YSZ electrode, similar trends were observed in the whole temperature range studied.

Tafel parameters were determined from polarization curves for various hydrogen and steam partial pressures and various temperatures, following

$$i = i_o(\exp^{\alpha_+\eta F/RT} - \exp^{-\alpha_-\eta F/RT}) \qquad [2]$$

where i, i_o are the current density and exchange current density, respectively, η is electrode overpotential, F, R, and T have their usual meanings, and α_+ and α_- are the charge transfer coefficients for the anodic and cathodic Tafel lines, respectively. Charge transfer coefficients for the Ni/YSZ electrode are given in Fig. 7 as a function of p_{H_2O} at different temperatures, for a constant p_{H_2} of 0.1 atm. In the SOFC direction, charge transfer coefficients were typically 1.1–1.3, and were independent of either temperature or p_{H_2O}. Charge transfer coefficients in the SOEC direction also varied little with either p_{H_2O} or temperature, but were consistently less than 0.5, indicating that the rate-determining step is less dependent on charge transfer. For the titanate/ceria composite electrode, charge transfer coefficients in the SOFC mode were ~0.6–0.7 and essentially independent of either p_{H_2O} or temperature, as shown in Fig. 8. In the SOEC direction, no dependence of charge transfer coefficients (~0.9 − 1) on p_{H_2O} was observed, although they did increase with increased temperature.

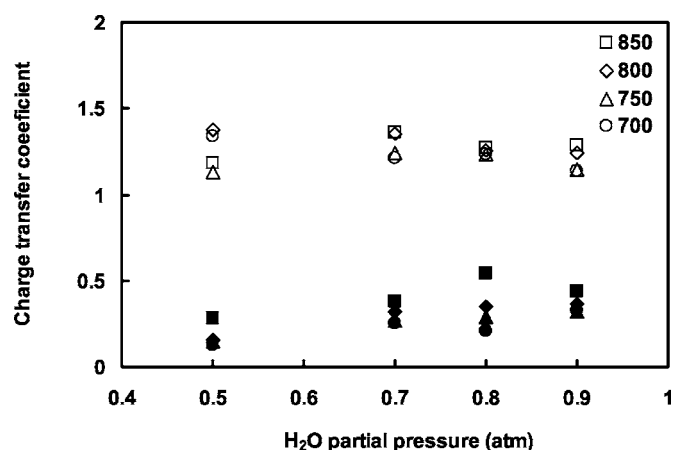Exchange current densities for Ni/YSZ and a titanate/ceria com-

Figure 7. Charge transfer coefficient calculated for the Ni/YSZ electrode in the SOFC (open symbols) and SOEC (closed symbols) modes as a function of steam partial pressure at 700–850°C and a partial pressure of hydrogen of 0.1 atm.

posite electrode are given in Fig. 9 and 10, respectively. Whereas exchange current densities for a titanate/ceria composite electrode were not affected by p_{H_2O} in either the SOFC or SOEC directions, results for the Ni/YSZ electrode showed an increasing dependence on p_{H_2O} with decreased temperature in the SOEC direction but no dependence in the SOFC direction. Because of differences in Tafel slopes in SOFC and SOEC modes for both electrodes, it is not useful to compare the magnitude of the exchange currents in the two directions. The temperature dependence of exchange current densities were used to obtain apparent activation energies for both electrodes in SOFC and SOEC directions, as shown in Fig. 11. For the Ni/YSZ electrode, activation energies of 0.7–0.9 and 0.9–1.3 eV were estimated for the anodic and cathodic curves, respectively, which increased with decreased p_{H_2O}. The obtained values of the apparent activation energy of hydrogen oxidation are in agreement with 0.7–1 eV that are typically reported on Ni/YSZ. A value of 2.0 eV for a Ni point electrode in contact with YSZ for steam electrolysis was reported by Olmer et al.[42] over the same temperature range. In contrast, the titanate/ceria electrode showed a noticeably lower activation energy and no p_{H_2O} dependence. Apparent activation energy of 0.5–0.7 eV was estimated for both hydrogen oxida-
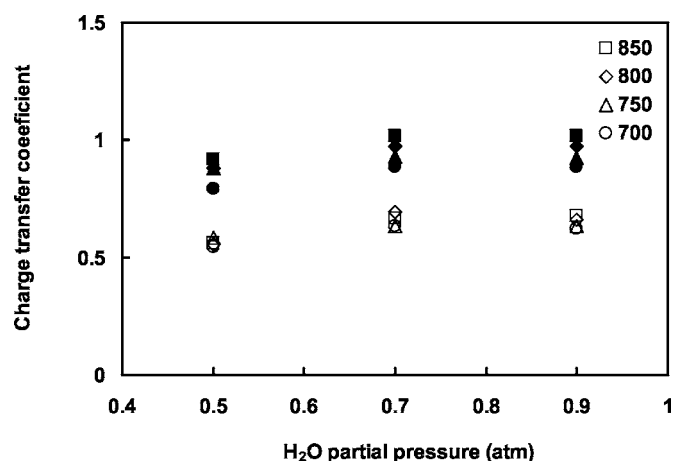

Figure 8. Charge transfer coefficient calculated for the titanate/ceria composite electrode in the SOFC (open symbols) and SOEC (closed symbols) modes as a function of steam partial pressure at 700–850°C and a partial pressure of hydrogen of 0.1 atm.
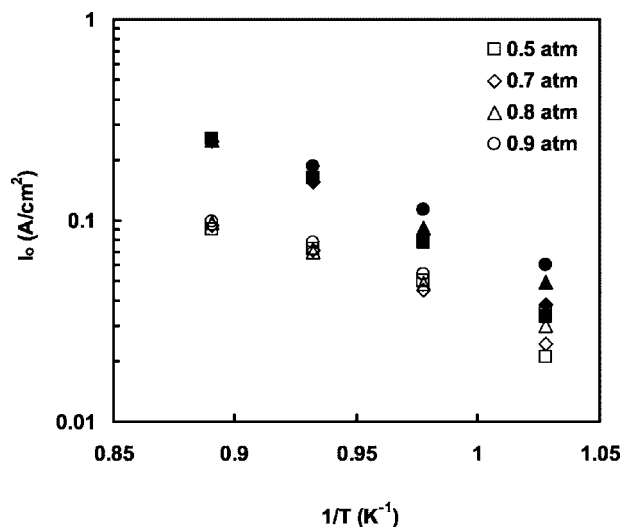
Figure 9. Exchange current densities of the Ni/YSZ electrode obtained at 850–700°C in the SOFC (open symbols) and SOEC (closed symbols) as a function of temperature. $p_{H_2} = 0.1$ atm.

Figure 11. Activation energies calculated from the temperature dependence of exchange current densities in the SOFC (open symbols) and SOEC (closed symbols) of Ni/YSZ (squares) and titanate/ceria (diamonds) as a function of pH_2O.

tion and steam electrolysis on the titanate/ceria electrodes under the experimental conditions studied. Thus, the activation energy of the reverse reaction appears to be higher on the Ni-YSZ electrode, while remaining unchanged for that on the titanate/ceria electrode.

When discussing electrode kinetics and determining the exchange current densities, we assumed that all of the measurements were performed in the absence of mass transport limitations. As seen in Fig. 5 and 6, the anodic dependencies for the Ni/YSZ electrode indeed obey the Butler-Volmer equation and are not transport limited. The cathodic curves of the Ni/YSZ electrode in turn deviate from the Butler-Volmer equation and exhibit a transport-controlled behavior. This could be attributed to the existence of a diffusion-limited process in the electrolysis direction. More experimental work is needed to clarify this behavior and determine the absolute values of i_o for the cathodic polarization region. However, in the present work the exchange current densities were only used to determine the temperature and p_{H_2O} trends and not for the comparison of absolute activities.

When operated at a high steam-to-hydrogen partial pressure of 90/10 for 100 h a significant activity loss was observed. It is believed due to significant microstructural changes, likely Ni particle coarsening/agglomeration at the triple-phase boundary. Eguchi et al.[14] also observed a Ni/YSZ activity loss when operated at high steam concentrations, $H_2O/H_2 = 10$. They have suggested that high steam and low hydrogen concentrations could lead to the Ni surface oxidation followed by an electrode activity drop.

Positive electrode polarization studies.— Current density vs overpotential for LSM-20, LSF-20, LSCuF-7319, and LSCoF-6428 are given in Fig. 12-15, respectively, for the temperature range 650–850°C. It is seen that electrode losses were generally higher under anodic (oxygen anion oxidation) than cathodic polarization (oxygen reduction). Of these compositions, the greatest differences between anodic and cathodic losses were observed for LSCuF-7319, and LSCuF-6428 whereas the least difference was found for LSM-20 and LSF-20. Because of variations in the sintered microstructure among positive electrode compositions considered, it is not particularly useful to rank the absolute activity of the positive electrodes. Rather, the relative activities of positive electrodes under
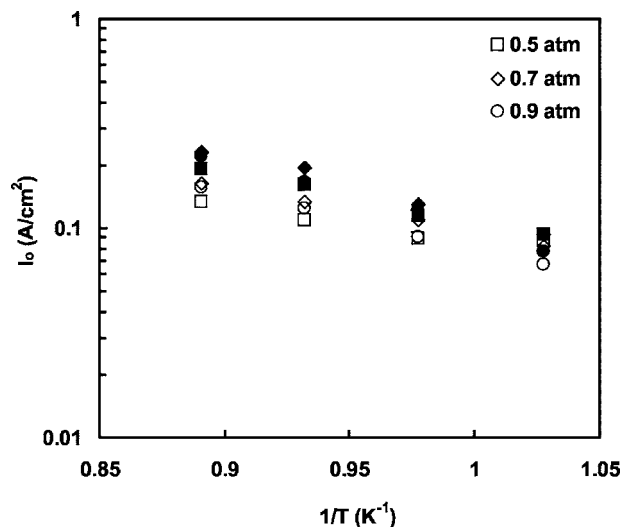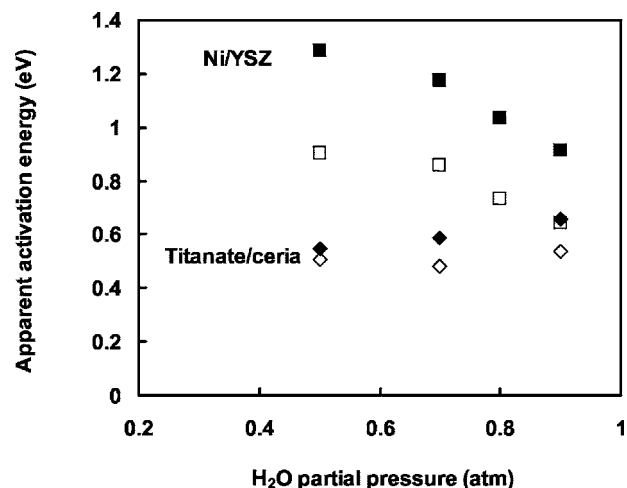

Figure 10. Exchange current densities of the titanate/ceria composite obtained at 850–700°C in the SOFC (open symbols) and SOEC (closed symbols) as a function of temperature. $p_{H_2} = 0.1$ atm.
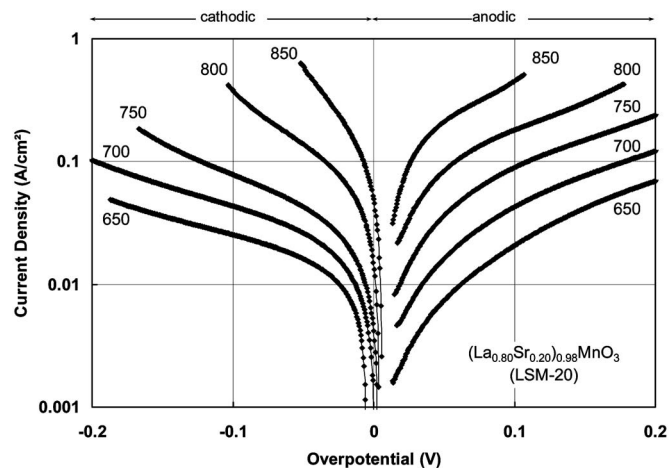

Figure 12. Cathodic and anodic overpotentials vs current density for LSM-20 on YSZ with a 3 μm thick SDC interlayer. The scan rate for this and subsequent figures was 0.1.
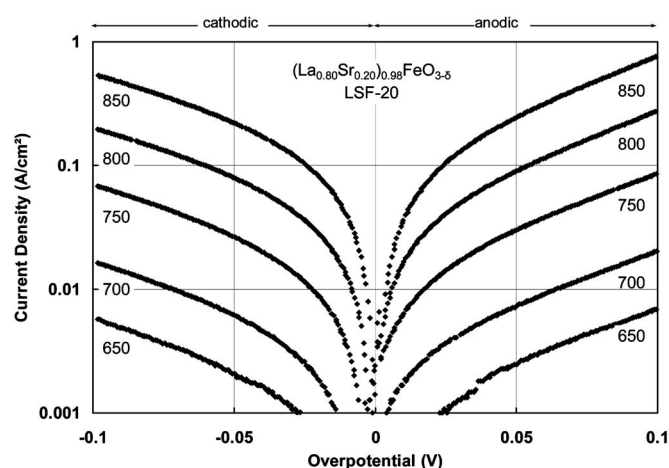
Figure 13. Cathodic and anodic overpotentials vs current density for LSF-30 on YSZ with a 3 μm thick SDC interlayer.

Figure 15. Cathodic and anodic overpotentials vs current density for LSCoF-6428 on YSZ with a 3 μm thick SDC interlayer.

cathodic and anodic polarization are considered to be more meaningful. Especially for compositions exhibiting significant mixed conduction, lower anodic activity is consistent with depletion of oxygen vacancies at the positive electrode/electrolyte interface.

Of the positive electrode compositions examined, LSM-20 and LSF-20 showed the smallest differences in polarization losses under cathodic and anodic polarization, Fig. 12, similar to results for LSM reported by Eguchi et al.[14] Tafel-like behavior was apparent in both directions, though current densities rose more steeply with cathodic polarization loss for $T > 800°C$. Oxygen in LSM has been shown to be nearly stoichiometric over a wide oxygen partial pressure range, from approximately 10^{-2} to 10^{-10} atm, and higher than stoichiometric for oxygen partial pressures greater than 10^{-2} atm.[43,44] Oxygen vacancy concentrations in LSM are very low, so mixed conductivity contributes minimally to the activity of LSM electrodes.[45-49] For example, oxygen ion conduction at 1000°C in oxygen partial pressures ranging from 10^{-1} to 10^{-3} atm has been reported to be 6×10^{-8} S/cm for LSM-10,[50] compared to a typical electronic component of greater than 200 S/cm. Although oxygen vacancy concentrations are very low, cathodic polarization of an LSM electrode on YSZ has been reported to affect both the oxygen stoichiometry and the activity of the electrode.[46,51,52] Furthermore, the lattice parameter of LSM electrodes was demonstrated to cycle reversibly with cathodic overpotential.[52]
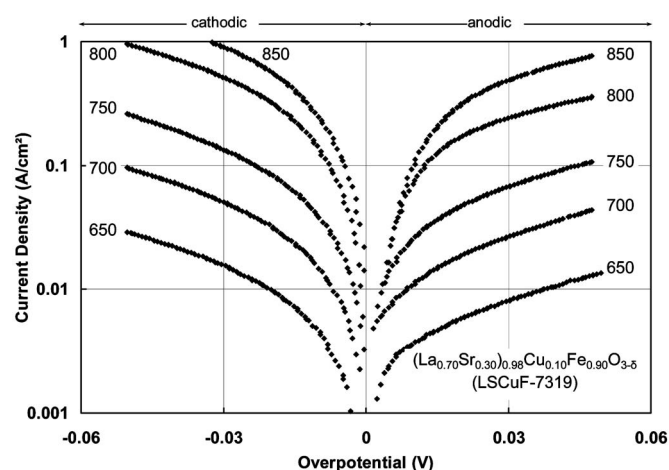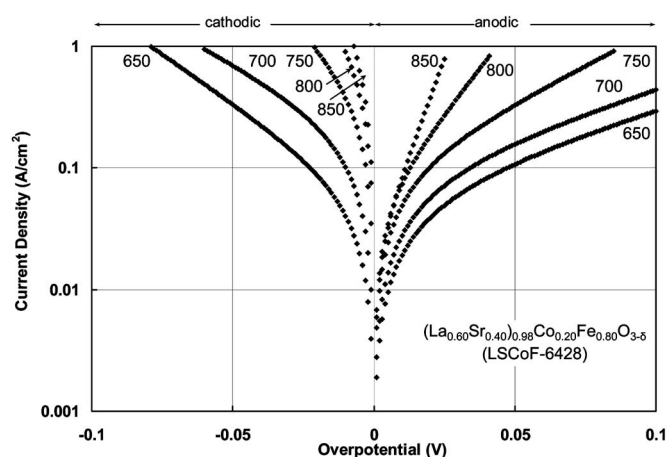
Greater asymmetry in performance under cathodic and anodic polarization was apparent for LSCuF-7319 and LSCoF-6428, Fig. 14 and 15, respectively. Results for LSCuF-7319, Fig. 14, most closely resemble predictions of a model for mixed conducting positive electrodes described by Svensson et al.[18] In that model, depletion of oxygen vacancies in the interfacial region leads to a limiting anodic current, whereas the production of oxygen vacancies under cathodic polarization results in currents rising faster with overpotential than expected for Tafel behavior. A comparison of Fig. 13 and 14 shows that partial substitution of copper for iron leads to higher cathodic activity and greater cathodic vs anodic asymmetry. Copper is primarily divalent in LSCuF compositions, resulting in effectively greater levels of acceptor doping as well as higher oxygen nonstoichiometry.[53,54] For LSCoF-6428, polarization losses were relatively low in both directions, although clearly lower in the cathodic direction. Current density limitations imposed by the use of a cell design with a thick electrolyte prevented attainment of a limiting slope, especially for temperatures $> 700°C$.

Mixed conductors such as substituted lanthanum ferrites and cobaltites exhibit oxygen vacancy concentrations and ion mobilities orders of magnitude higher than those of LSM.[49,55-57] These highly active electrodes enable SOFCs to be operated at temperatures lower than possible with LSM cathodes. In contrast to LSM, LSF is slightly oxygen-deficient in air;[58,59] LSCoF[60] and LSCuF[53,54] show higher levels of oxygen nonstoichiometry. High mixed conductivity is at least partially responsible for high activity as the oxygen electrode in an SOFC.[61] As such, when oxygen vacancies are depleted at the high local oxygen partial pressures that are produced under anodic polarization, mixed conductivity as well as electrocatalytic performance will be diminished.

No attempt was made to correct polarization curves for a small Nernstian off-set potential that could have contributed to apparent anodic polarization losses. For the anodic reaction, despite the fact that an airflow was maintained across the electrode surface, nearly pure oxygen may exist at the electrode/electrolyte interface, whereas the reference electrode was maintained in air. In the worst case, this Nernstian off-set could add up to 32 mV at 650°C and up to 38 mV at 850°C to apparent anodic polarization losses, which is still small compared to the difference between cathodic and anodic performance of the positive electrode.

Comparison of stack operation as an SOFC and SOEC.— A single anode-supported cell with an active area of 33.6 cm², a Ni/YSZ negative electrode, a 7 μm thick YSZ electrolyte, a 2 μm thick SDC barrier layer, and an LSCoF-6428 positive electrode, was operated at 750°C as both a fuel cell and steam electrolyzer. Three different hydrogen-to-steam ratios, 10/90, 50/50, and 90/10, were used in the SOEC mode, while a 97/3 hydrogen-to-steam mixture
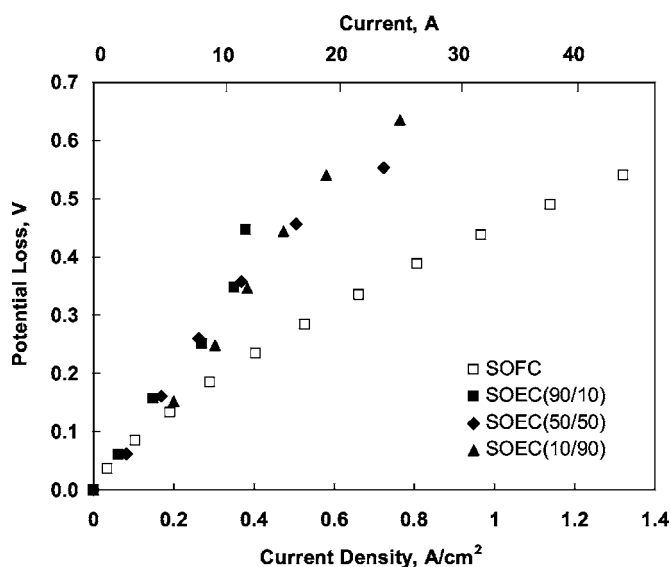

Figure 14. Cathodic and anodic overpotentials vs current density for LSCuF-7319 on YSZ with a 3 μm thick SDC interlayer.

Figure 16. Potential losses vs current density for an Ni/YSZ-supported single cell operated in SOFC (open symbols) and SOEC (closed symbols, H_2/H_2O = 90/10, 50/50, and 10/90) at 750°C, corrected for initial steam/hydrogen concentrations and reaction.

was used in the SOFC mode. Figure 16 provides potential losses as a function of current density, corrected for different open circuit potential as well as gas conversion (reaction). It is seen that higher cell resistances were obtained in the electrolyzer than fuel cell direction that is consistent with electrode polarization results obtained using half-cells. Steam electrolysis results were similar over a wide range of steam partial pressures, but clearly show higher resistances than obtained for fuel cell operation, especially at the highest current densities.

Conclusions

As part of the development of a reversible solid oxide fuel cell that can alternately produce hydrogen fuel and electricity, the anodic and cathodic polarization of several negative and positive electrode compositions have been studied. Titanate-ceria electrodes were found to be more active than standard Ni/YSZ compositions for steam electrolysis, whereas the two electrodes show similar activity as the anode in a solid oxide fuel cell. The performance of a titanate/cerate composite electrode was enhanced by high hydrogen partial pressures and diminished by high steam partial pressures, although any loss in activity could be recovered by returning to more favorable conditions. This behavior is at least partially attributable to a loss in electrical conductivity of the ceramic composite under relatively oxidizing conditions. Particularly under high steam and low hydrogen partial pressures, the Ni/YSZ electrode underwent irreversible degradation. Although promising, further lifetime testing of the ceramic composite electrodes is needed to demonstrate potential viability.

Positive electrodes generally performed less well for oxygen evolution than oxygen reduction. This behavior was most apparent for mixed-conducting LSCuF and LSCoF electrodes, while the effect was less but still discernable for LSM. These observations are consistent with an expected decrease in the oxygen vacancy concentration as one proceeds from cathodic to anodic polarization.

Higher resistances were obtained for an anode-supported, thin electrolyte cell in the electrolysis than fuel cell directions, consistent with half-cell studies. Similar current-voltage characteristics were obtained in the SOEC mode for a wide range of steam concentrations, after adjusting for the open-cell potential and steam concentrations. Although the contributions of each electrode were not indi-

vidually assessed in the full cell, it is expected that the performance of the positive electrode dominated overall performance.

References

1. N. J. Maskalick, *Int. J. Hydrogen Energy*, **11**, 563 (1986).
2. J. A. Turner, M. C. Williams, and K. Rajeshwar, *Electrochem. Soc. Interface*, **13**, 24 (2004).
3. E. D. Wachsman and M. C. Williams, *Electrochem. Soc. Interface*, **13**, 32 (2004).
4. National Research Council and National Academy of Engineering. *The Hydrogen Economy-Opportunities, Costs, Barriers, and R&D Needs*, The National Academies Press, www.nap.edu, Washington, D.C., 2004.
5. U.S. Department of Energy and Office of Energy Efficiency and Renewable Energy, Hydrogen Fuel Cells and Infrastructure Technologies Program: Multi-Year Research, Development and Demonstration Plan, 2003.
6. R. Hino, K. Haga, H. Aita, and K. Sekita, *Nucl. Eng. Des.*, **233**, 363 (2004).
7. *Fuel Cell Handbook*, U.S. Department of Energy, Washington, DC (2004).
8. J. E. O'Brien, C. M. Stoots, J. S. Herring, and J. Hartvigsen, in *FUELCELL2005*, p. 1, Ypsilanti, MI (2005).
9. E. Erdle, W. Donitz, R. Schamm, and A. Koch, *Int. J. Hydrogen Energy*, **17**, 817 (1992).
10. W. Doenitz, R. Schmidberger, E. Steinheil, and R. Streicher, *Int. J. Hydrogen Energy*, **5**, 55 (1980).
11. W. Doenitz and R. Schmidberger, *Int. J. Hydrogen Energy*, **7**, 321 (1982).
12. W. Donitz and E. Erdle, *Int. J. Hydrogen Energy*, **10**, 291 (1985).
13. W. Donitz, G. Dietrich, E. Erdle, and R. Streicher, *Int. J. Hydrogen Energy*, **13**, 283 (1988).
14. K. Eguchi, T. Hatagishi, and H. Arai, *Solid State Ionics*, **86**, 1245 (1996).
15. A. Momma, T. Kato, Y. Kaga, and S. Nagata, *J. Ceram. Soc. Jpn.*, **105**, 369 (1997).
16. A. Hauch, S. H. Jensen, and M. Mogensen, in *Proceedings of the 26th Risoe International Symposium on Materials Science: Solid State Electrochemistry*, S. Linderoth, A. Smith, N. Bonanos, A. Hagen, L. Mikkelsen, K. Kammer, D. Lybye, P. V. Hendriksen, F. W. Poulsen, M. Mogensen, and W. G. Wang, Editors, p. 203, Roskilde, Denmark (2005).
17. T. Jacobsen, B. Zachau-Christiansen, L. Bay, and M. J. Jorgensen, *Electrochim. Acta*, **46**, 1019 (2001).
18. A. M. Svensson, S. Sunde, and K. Nisancioglu, *J. Electrochem. Soc.*, **145**, 1390 (1998).
19. J. E. O'Brien, C. M. Stoots, J. S. Herring, P. A. Lessing, J. J. Hartvigsen, and S. Elangovan, *J. Fuel Cell Sci. Technol.*, **2**, 156 (2005).
20. O. A. Marina, N. L. Canfield, and J. W. Stevenson, *Solid State Ionics*, **149**, 21 (2002).
21. S. Q. Hui and A. Petric, *Mater. Res. Bull.*, **37**, 1215 (2002).
22. S. Q. Hui and A. Petric, *J. Eur. Ceram. Soc.*, **22**, 1673 (2002).
23. J. Canales-Vazquez, S. W. Tao, and J. T. S. Irvine, *Solid State Ionics*, **159**, 159 (2003).
24. G. Pudmich, B. A. Boukamp, M. Gonzalez-Cuenca, W. Jungen, W. Zipprich, and F. Tietz, *Solid State Ionics*, **135**, 433 (2000).
25. O. A. Marina and L. R. Pederson, in *Proceedings of the 5th European Solid Oxide Fuel Cell Forum*, Vol. 1, J. Huijsmans, Editor, p. 481, Lucerne, Switzerland (2002).
26. O. A. Marina, J. W. Stevenson, and L. R. Pederson, Paper presented at the Fuel Cell Seminar, San Antonio, TX, November 1-5, 2004.
27. M. R. Deguire, M. J. Shingler, and E. Dincer, *Solid State Ionics*, **52**, 155 (1992).
28. S. P. Simner, J. F. Bonnett, N. L. Canfield, K. D. Meinhardt, V. L. Sprenkle, and J. W. Stevenson, *Electrochem. Solid-State Lett.*, **5**, A173 (2002).
29. S. P. Simner, J. P. Shelton, M. D. Anderson, and J. W. Stevenson, *Solid State Ionics*, **161**, 11 (2003).
30. S. P. Simner, J. R. Bonnett, N. L. Canfield, K. D. Meinhardt, J. P. Shelton, V. L. Sprenkle, and J. W. Stevenson, *J. Power Sources*, **113**, 1 (2003).
31. S. Tanasescu, N. D. Totir, and D. I. Marchidan, *Solid State Ionics*, **119**, 311 (1999).
32. J. E. Tenelshof, H. J. M. Bouwmeester, and H. Verweij, *Solid State Ionics*, **81**, 97 (1995).
33. J. E. tenElshof, H. J. M. Bouwmeester, and H. Verweij, *Solid State Ionics*, **89**, 81 (1996).
34. J. E. tenElshof, M. H. R. Lankhorst, and H. J. M. Bouwmeester, *J. Electrochem. Soc.*, **144**, 1060 (1997).
35. G. W. Coffey, J. S. Hardy, O. A. Marina, L. R. Pederson, and E. C. Thomsen, *Solid State Ionics*, **175**, 73 (2004).
36. J. M. Ralph, J. T. Vaghey, and M. Krumpelt, in *Solid Oxide Fuel Cells VII*, J. Yokokawa and S. C. Singhal, Editors, PV 2001-16, p. 466, The Electrochemical Society Proceedings Series, Pennington, NJ (2001).
37. L. A. Chick, L. R. Pederson, G. D. Maupin, J. L. Bates, L. E. Thomas, and G. J. Exarhos, *Mater. Lett.*, **10**, 6 (1990).
38. G. Hsieh, T. O. Mason, E. J. Garboczi, and L. R. Pederson, *Solid State Ionics*, **96**,

153 (1997).

39. S. Mukerjee, S. Shaffer, J. Zizelman, L. A. Chick, S. Baskaran, Y.-S. Chou, C. A. Coyle, J. E. Deibler, G. D. Maupin, K. D. Meinhardt, D. M. Paxton, T. J. Peters, V. L. Sprenkle, K. S. Weil, and R. E. Williford, in *Solid Oxide Fuel Cells VIII*, S. C. Singhal and M. Dokia, Editors, PV 2003-07, p. 89, The Electrochemical Society Proceedings Series, Pennington, NJ (2003).

40. J. Sehested, *Catal. Today*, **111**, 103 (2006).

41. O. A. Marina and J. W. Stevenson, in *Solid State Ionic Devices III*, E. D. Wachsman, K. Swider-Lyons, M. F. Carolan, F. H. Garzon, M. Liu, and J. R. Stetter, Editors, PV 2002-26, p. 91, The Electrochemical Society Proceedings Series, Pennington, NJ (2002).

42. L. J. Olmer, J. C. Viguie, and E. J. L. Schouler, *Solid State Ionics*, **7**, 23 (1982).

43. J. H. Kuo, H. U. Anderson, and D. M. Sparlin, *J. Solid State Chem.*, **83**, 52 (1989).

44. J. H. Kuo, H. U. Anderson, and D. M. Sparlin, *J. Solid State Chem.*, **87**, 55 (1990).

45. R. Radhakrishnan, A. V. Virkar, and S. C. Singhal, *J. Electrochem. Soc.*, **152**, A210 (2005).

46. F. W. Poulsen, *Solid State Ionics*, **129**, 145 (2000).

47. J. Mizusaki, T. Saito, and H. Tagawa, *J. Electrochem. Soc.*, **143**, 3065 (1996).

48. V. Brichzin, J. Fleig, H. U. Habermeier, G. Cristiani, and J. Maier, *Solid State Ionics*, **152**, 499 (2002).

49. R. A. De Souza and J. A. Kilner, *Solid State Ionics*, **106**, 175 (1998).

50. A. Endo, M. Ihara, H. Komiyama, and K. Yamada, *Solid State Ionics*, **86–88**, 1191 (1996).

51. E. Siebert, A. Hammouche, and M. Kleitz, *Electrochim. Acta*, **40**, 1741 (1995).

52. L. Sorby, F. W. Poulsen, H. F. Poulsen, S. Garbe, and J. O. Thomas, *Mater. Sci. Forum*, **278**, 408 (1998).

53. G. J. Long, D. Hautot, A. Mohan, I. Kaus, H. U. Anderson, and F. Grandjean, *J. Appl. Phys.*, **85**, 5341 (1999).

54. I. Kaus and H. U. Anderson, *Solid State Ionics*, **129**, 189 (2000).

55. J. M. Bae and B. C. H. Steele, *Solid State Ionics*, **106**, 247 (1998).

56. J. A. Lane, S. J. Benson, D. Waller, and J. A. Kilner, *Solid State Ionics*, **121**, 201 (1999).

57. J. Yoo, A. Verma, S. Y. Wang, and A. J. Jacobson, *J. Electrochem. Soc.*, **152**, A497 (2005).

58. J. Mizusaki, T. Sasamoto, W. R. Cannon, and H. K. Bowen, *J. Am. Ceram. Soc.*, **66**, 247 (1983).

59. J. Mizusaki, M. Yoshihiro, S. Yamauchi, and K. Fueki, *J. Solid State Chem.*, **58**, 257 (1985).

60. H. Wendt and V. Plzak, *Kerntechnik*, **56**, 22 (1991).

61. J. Fleig, *Annu. Rev. Mater. Res.*, **33**, 361 (2003).